Dynamic Fluctuations and Spatial Inhomogeneities in Poly(*N*-isopropylacrylamide)/Clay Nanocomposite Hydrogels Studied by Dynamic Light Scattering

Jingjing Nie, Binyang Du, and Wilhelm Oppermann*

Institute of Physical Chemistry, Clausthal University of Technology, Arnold-Sommerfeld Strasse 4, 38678 Clausthal-Zellerfeld, Germany

Received: October 13, 2005; In Final Form: January 30, 2006

The contributions of the dynamic fluctuations and the frozen-in inhomogeneities to the total light scattering intensity observed in poly(*N*-isopropylacrylamide)/clay nanocomposite hydrogels were analyzed by applying the nonergodic method proposed by Pusey and van Megen. Approximately 90% of the total scattering intensity corresponds to the frozen-in component. The scattering intensity of the fluctuating component is smaller by far than that of a pure clay suspension, indicating that the thermal fluctuations of the clay particles are largely suppressed upon network formation. Accordingly, the fluctuating component consists of two contributions: one due to the polymer chains and the other, smaller one representing the residual mobility of the clay particles. The latter depends on how tightly the clay particles are fixed in the network. The dynamic features of the nanocomposite hydrogels are described by two relaxation modes. The fast one is purely diffusive and can be related to a dynamic correlation length of 6−8 nm, which is similar to that of a corresponding polymer solution. The relaxation time of the slow mode varies appreciably with sample position even though the data had been treated with the nonergodic method.

Introduction

Polymer hydrogels are three-dimensional networks which swell in an aqueous solution. If suitable monomers are chosen, the resulting hydrogels can be sensitive or responsive to various external stimuli, such as temperature,[1] ionic strength,[2] pH value,[3] etc. It is because of such functionalities that hydrogels are sometimes called "smart materials"[4] and thought to have potential applications in controlled drug release,[5] in gene delivery,[6] or as sensors.[7] Most practical applications of hydrogels depend decisively on their macroscopic physical properties, in particular, the elasticity and swelling behavior, which in turn are governed by their structural and chemical peculiarities. Understanding and controlling the structural inhomogeneities of hydrogels are some of the key issues for their actual performance.[8] This topic has attracted great attention in polymer science for some decades, and the influence of the preparation conditions on the structural inhomogeneities as well as on the macroscopic physical properties has been elucidated for a number of different types of hydrogels.[9−20]

In the past, the most attention was paid to the investigation of chemically cross-linked hydrogels, commonly prepared by free radical copolymerization of a monomer with a cross-linker such as *N*,*N*′-methylene bis(acrylamide) (BIS). However, poor mechanical properties of the traditional chemically cross-linked hydrogels (brittleness, low elongation at break) make them difficult to handle and process, which largely limits their real applications. To improve the mechanical properties, several research groups recently reported on the incorporation of inorganic components into the gel systems in the formation of inorganic−organic nanocomposite hydrogels.[21−29]

A special type of inorganic−organic nanocomposite hydrogel is obtained when the thermosensitive monomer *N*-isopropyl acrylamide (NIPA) is polymerized without any chemical cross-linkers in the presence of nanosized synthetic clay particles (Laponite).[24,25,28,29] The preparation of such systems was reported first by Haraguchi et al.[24,25] These authors used Laponite XLG particles (a special preparation of synthetic clay), which are exfoliated to form a uniformly dispersed aqueous suspension and act as multifunctional cross-links in the hydrogels. Due to strong interactions at the clay−polymer interface, permanent nanocomposite hydrogels were formed without cross-linking via covalent chemical bonds. Not only the mechanical and swelling−deswelling properties but also the spatial homogeneities of the nanocomposite gels were markedly improved. Such nanocomposite gels are believed to have a wide range of potential applications.

Haraguchi et al.[30] reported that the PNIPA/Laponite XLG nanocomposite hydrogel could only be realized by in situ free radical polymerization of NIPA in the presence of clay. Mixing of the clay with a solution of the polymer or in situ polymerization in the presence of other inorganic nanoparticles did not lead to hydrogels with excellent mechanical properties and structural homogeneity. These observations raise questions regarding the interactions between clay and the growing polymer chains as well as questions about which monomers and nanoparticles can lead to similar features. A second major challenge is the elucidation of the network microstructure, the spatial inhomogeneity, and the chain dynamics in such nanocomposite hydrogels.

With regard to microstructure and its dependence on the preparation conditions of the nanocomposite hydrogels, we reported earlier that two levels of organization, characterized by two correlation lengths, were observed in PNIPA/Laponite RDS hydrogels.[29] (We used Laponite RDS, which is different from Laponite XLG in that the edges of the clay platelets are modified to achieve a negative surface charge.) The smaller correlation length is on the same order of magnitude as that

* To whom correspondence should be addressed. E-mail: wilhelm.oppermann@tu-clausthal.de.

10.1021/jp055853y CCC: $33.50
Published on Web 05/18/2006

observed in chemically cross-linked gels. It also shows the same tendency with varying preparation conditions, such as monomer concentration, clay concentration, and preparation temperature. The larger correlation length, however, is a peculiarity of the nanocomposite hydrogels. Being around 200 nm, essentially independent of the preparation conditions, it is thought to be due to the formation of large-scale structures resulting from a kinetically controlled rearrangement of clay particles when more and more network chains are attached to them in a stepwise manner.

Moreover, the chain dynamics and the microstructure of PNIPA/Laponite XLG hydrogels were investigated by Shibayama et al.[28] using small-angle neutron scattering (SANS) and dynamic light scattering (DLS). Their study shows that the chain dynamics are similar to those of conventional chemically cross-linked PNIPA hydrogels.

In this work, we further extended our investigations of the spatial inhomogeneities and dynamic fluctuations of PNIPA/Laponite RDS nanocomposite hydrogels by performing DLS measurements as a function of clay concentration and monomer concentration. The results are discussed in connection with those of previous static light scattering (SLS) measurements on the same systems[29] and furthermore compared with those observed with conventional chemically cross-linked hydrogels. It is found that the dynamic fluctuations of the clay particles are largely suppressed after the formation of the nanocomposite hydrogels. In addition, the differences in dynamic fluctuation between nanocomposite hydrogels and pure clay suspensions are discussed.

Theoretical Background

DLS is a suitable experimental technique for investigating the dynamic properties of polymer systems on a variety of length scales. Cross-linked systems, however, pose a particular challenge because of their nonergodic nature. To overcome the complications attributed to this fact, and to extract reliable and fundamental information, different methods of measurement and data analysis have been proposed, such as the nonergodic method, the partial heterodyne method, and the homodyne method.[31−37] Thereby, the contributions of the dynamic fluctuations and the frozen-in inhomogeneities to the total scattered intensity are successfully separated. DLS experiments can then simultaneously provide information about the dynamic fluctuations and the frozen-in inhomogeneities of hydrogels.

In this work, we applied the nonergodic method proposed by Pusey and van Megen.[31] In the following, we give a very brief summary of its basic elements and present the main equations used to analyze the experimental data.

The amplitude $[E(q,t)]$ of the electric field of light scattered by a medium undergoing fluctuations $[\rho(r,t)]$ in concentration at time t can be written as[38]

$$E(q,t) \sim \rho(q,t) = \int_v \mathrm{d}^3 r\, \rho(r,t) \exp(iqr) \tag{1}$$

where $q = (4\pi n/\lambda)\sin(\theta/2)$ is the amplitude of the scattering vector with θ being the scattering angle, n the refractive index of the medium, and λ the wavelength of the incident light in a vacuum.

The scattered intensity as determined by light scattering experiments is

$$I(q,t) = |E(q,t)|^2 \tag{2}$$

In a single DLS experiment, one determines the (normalized) time-averaged intensity autocorrelation function (ICF) $g_T^{(2)}(q,\tau)$ of the scattered intensity given as

$$g_T^{(2)}(q,\tau) = \frac{\langle I(q,0)I(q,\tau)\rangle_T}{\langle I(q,0)\rangle_T^2} \tag{3}$$

where τ denotes time and $\langle ...\rangle_T$ means a time average. For an ergodic system, the scattered intensity contains only a fluctuating component, i.e., $\langle I(q,t)\rangle_T = \langle I_F(q,t)\rangle_T = \langle |E_F(q,t)|^2\rangle_T$, where $E_F(q,t)$ is a zero-mean complex Gaussian variable in the time domain and independent of position. $g_T^{(2)}(q,\tau)$ is then equivalent to an ensemble-averaged ICF, $g_E^{(2)}(q,\tau)$, and can be related to the normalized scattering function or dynamic structure factor $g_T^{(1)}(q,\tau)$ via the Siegert relation[38]

$$g_T^{(2)}(q,\tau) = g_E^{(2)}(q,\tau) = \frac{\langle I(q,0)I(q,\tau)\rangle_E}{\langle I(q,0)\rangle_E^2} = 1 + \beta |g_T^{(1)}(q,\tau)|^2 \tag{4}$$

where β is the coherence factor of the instrument and $\langle ...\rangle_E$ indicates an ensemble average over all possible configurations of the medium. However, for a system containing an infinite network or having a "frozen-in" structure, the scattered intensity also contains another contribution, i.e., the frozen-in (or static) component, viz. $\langle I(q,t)\rangle_T = \langle I_F(q,t)\rangle_T + I_C(q)$ and $I_C(q) = |E_C(q)|^2$. The frozen-in (or static) component $I_C(q)$ is independent of time but depends on the position of the scattering volume within the sample. Regions at different locations in one sample scatter differently, a fact leading to the so-called "speckle pattern" in DLS measurements. In this case, the Siegert relation (eq 4) does not hold. According to Pusey and van Megen, $g_T^{(2)}(q,\tau)$ can then be expressed as[31]

$$g_T^{(2)}(q,\tau) - 1 = \frac{\langle E_F(q,0)E_F^*(q,\tau)\rangle_T^2 + 2I_C(q)\langle E_F(q,0)E_F^*(q,\tau)\rangle_T}{\langle I(q,0)\rangle_T^2} \tag{5}$$

For an arbitrary nonergodic medium, it was shown that

$$\langle E_F(q,0)E_F^*(q,\tau)\rangle_T = \langle E_F(q,0)E_F^*(q,\tau)\rangle_E = \langle I(q)\rangle_E[f(q,\tau) - f(q,\infty)] \tag{6}$$

where $f(q,\tau)$ is the normalized intermediate ensemble-averaged scattering function given by

$$f(q,\tau) = \frac{\langle \rho(q,0)\rho^*(q,\tau)\rangle_E}{\langle |\rho(q)|^2\rangle_E} \tag{7}$$

[We use the letter f to clearly distinguish the intermediate scattering function of a nonergodic medium from the dynamic structure factor $g^{(1)}$ of an ergodic medium.]

The zero-time limit of eq 6 gives

$$\langle I_F(q)\rangle_T = \langle I_F(q)\rangle_E = \langle I(q)\rangle_E[1 - f(q,\infty)] \tag{8}$$

Using eqs 6 and 8 and considering the coherence factor β, $f(q,\tau)$ can be solved from eq 5:[32,39]

$$f(q,\tau) = 1 + \frac{\langle I(q)\rangle_T}{\langle I(q)\rangle_E}\left[\sqrt{\frac{g_T^{(2)}(q,\tau) - 1 - \sigma_I^2}{\beta}} + 1 - 1\right] \tag{9}$$

where $\sigma_I^2 = g_T^{(2)}(q,0) - 1$ is the initial amplitude of the time-averaged ICF.

In summary, we realize that the normalized intermediate ensemble-averaged scattering function, $f(q,\tau)$, can be directly calculated with eq 9 from a single time-averaged ICF, $g_T^{(2)}(q,\tau)$, provided that $\langle I(q)\rangle_E$ was also obtained. $f(q,\tau)$ values calculated from different $g_T^{(2)}(q,\tau)$ values characterizing different sample positions should be identical for a given system.

Experimental Section

Sample Preparation. *N*-Isopropylacrylamide (NIPA, ACROS), potassium peroxodisulfate ($K_2S_2O_8$, Sigma), and *N*,*N*,*N*′,*N*′-tetramethylethylenediamine (TEMED, Sigma) were used as received. The synthetic hectorite clay, Laponite RDS $\{Na^+_{0.7}[(Si_8Mg_{5.5}Li_{0.3})O_{20}(OH)_4]^{0.7-}$, modified with pyrophosphate ions ($P_2O_7^{4-}$)}, was kindly provided by Rockwood Ltd. Suspensions of Laponite RDS were newly prepared right before being used by dispersing the white powder at the preset concentrations in deionized water with vigorous stirring for at least 1 h. The PNIPA/Laponite RDS nanocomposite hydrogels were prepared as described previously.[29] Briefly, PNIPA/Laponite RDS hydrogels were prepared by free radical polymerization of NIPA in an aqueous RDS suspension. Corresponding solutions of the linear polymer were obtained by free radical polymerization under identical conditions in the absence of Laponite RDS. Potassium peroxodisulfate ($K_2S_2O_8$) and *N*,*N*,*N*′,*N*′-tetramethylethylenediamine (TEMED) were used as the initiator and accelerator, respectively. The solutions and the gel samples were prepared in light scattering vials having an inner diameter of 8 mm. Dust was removed from the solutions when they were filtered through Nylon membrane filters with a pore size of 0.2 μm prior to the reaction. Two series of gels, in which the monomer concentration or the clay concentration was varied systematically and the other parameters were kept fixed, were prepared. All samples were prepared at 25 °C in a water bath.

Dynamic Light Scattering (DLS) measurements were performed at 25 °C in the angular range of 40−150° with steps of 10° using an ALV/CGS-3 compact goniometer (ALV, Langen, Germany) equipped with a cuvette rotation/translation unit (CRTU) and a He−Ne laser (22 mW, wavelength λ of 632.8 nm). A fiber optical detection unit based on three-mode detection was used, which includes an appropriate collimator/GRIN-lens fiber and the ALV/STATIC and DYNAMIC enhancer. Ideally, the three-mode detection unit gives an intercept in $g_T^{(2)}(q,0) - 1$ of 0.33; viz., β should be 0.33. An experimental check with a polystyrene latex suspension gave a coherence factor β of 0.36 ± 0.01, and this value was used for the evaluation of the DLS measurements. To protect the detector, the intensity of the incident light is automatically attenuated at each measurement by an eight-step automatic software-controlled attenuator and measured with a monitor diode. Thus, the intensity of incident light can be different within a series of measurements. When discussing scattering intensities, we therefore use data that were rescaled to a preset value of the monitor diode assuming a linear count rate dependence. Toluene was used as the index matching liquid. The temperature was controlled with an external thermostat. For each scattering angle, the time-averaged ICFs were acquired at 50 different sample positions, except for 90° which was acquired with 100 sample positions. The sample positions were selected by randomly moving the CRTU before each run. The acquisition time for each run was 40 s. The ensemble-averaged scattered intensity, $\langle I(q)\rangle_E$, was determined by continuously moving the sample vial with the CRTU, and the acquisition time for $\langle I(q)\rangle_E$ at every scattering angle was 3 min.

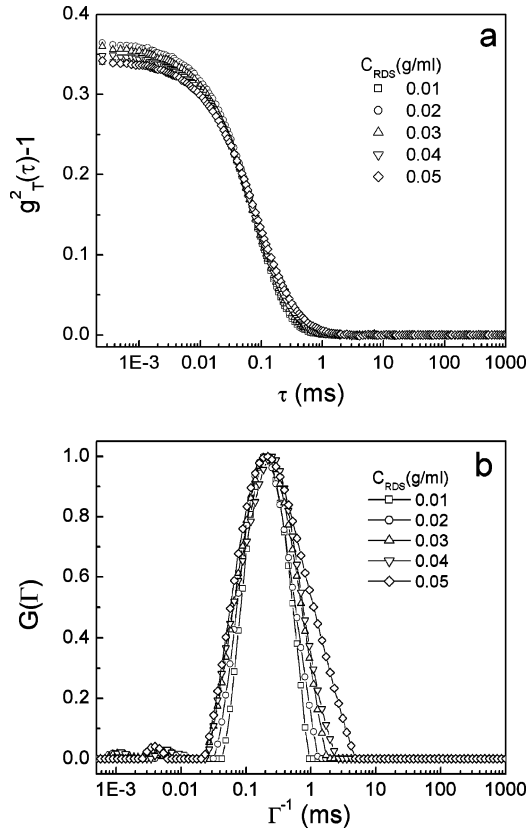

Figure 1. (a) Normalized time-averaged ICF, $g_T^{(2)}(\tau) - 1$, of Laponite RDS suspensions with various concentrations taken at a scattering angle of 90°. (b) Characteristic decay time distribution functions, $G(\Gamma)$, of the ICFs depicted in panel a.

Results and Discussion

1. Dynamics of Laponite RDS Suspensions and PNIPA Solutions. Before we discuss the dynamics of the PNIPA/Laponite RDS nanocomposite hydrogels, it is appropriate to obtain some view of the corresponding primary systems, i.e., pure Laponite RDS suspensions and PNIPA solutions. By static light scattering (SLS) measurements, we have previously shown that Laponite RDS forms a uniform aqueous suspension in the concentration range of 0.01−0.05 g/mL. This result is further confirmed in this work by DLS measurements.

Figure 1a shows the normalized time-averaged ICF, $g_T^{(2)}(q,\tau) - 1$, of pure Laponite RDS suspensions with various concentrations taken at $\theta = 90°$. Two observations can be directly pointed out. First, $g_T^{(2)}(q,\tau) - 1$ is almost the same for all clay suspensions regardless of the concentration; second, the initial amplitude σ_I^2 is close to the instrumental coherence factor β, indicating the ergodic character of the clay suspensions. For an ergodic system, the Siegert relation, eq 4, holds. The normalized dynamic structure factor $g_T^{(1)}(q,\tau)$ can be expressed as

$$g_T^{(1)}(q,\tau) = \int_0^\infty G(\Gamma)\exp(-\Gamma\tau)\,d\Gamma \qquad (10)$$

where $G(\Gamma)$ is the distribution function of the characteristic decay time Γ^{-1}. Figure 1b shows $G(\Gamma)$ values obtained with an inverse Laplace transform of $g_T^{(2)}(q,\tau) - 1$ with the integrated ALV software. Each $G(\Gamma)$ function has a significant peak at the same position, although $G(\Gamma)$ slightly broadens with an increase in the clay concentration. The value of decay time Γ^{-1} is related to hydrodynamic radius R_h of clay particles via the Stokes−Einstein equation

$$R_h = \frac{k_B T}{6\pi\eta_s D} \tag{11}$$

where k_B is the Boltzmann constant, T is the absolute temperature, η_s is the solvent viscosity (here $\eta_s = 0.89$ mPa for water), and D (the diffusion coefficient) $= \Gamma/q^2$. The hydrodynamic radius of Laponite RDS obtained here by DLS, i.e., $R_h = 18$ nm, is in reasonable agreement with radii obtained by SLS[29] and small-angle X-ray scattering (SAXS).[40] The DLS results show that the clay particles are uniformly dispersed in the suspension, which is consistent with the SLS measurements.[29]

Panels a and b of Figure 2 show the $g_T^{(2)}(q,\tau) - 1$ values and the corresponding $G(\Gamma)$ values taken at $\theta = 90°$ for PNIPA solutions with different concentrations. Initial amplitude σ_I^2 is a little less than instrumental coherence factor β (Figure 2a), indicating a slight nonergodicity of PNIPA solutions. One may expect an ergodic behavior for a polymer solution. However, temporal cross-links may be formed via hydrophobic association of *N*-isopropyl groups in PNIPA solutions, which could lead to a gel-like behavior.[9,41,42] Each $G(\Gamma)$ exhibits a major fast relaxation mode and several minor slow ones, which are typically observed in semidilute polymer solutions. Compared with those of clay suspensions, the fast mode of PNIPA solutions gives a sharper peak. The fast mode shifts to shorter times with an increase in the PNIPA concentration. The results are reasonable since the concentrations of the PNIPA solutions used here are in the semidilute regime.

2. Dynamics of PNIPA/Laponite RDS Nanocomposite Hydrogels. The dynamics of PNIPA/Laponite RDS nanocomposite hydrogels were systematically investigated by DLS measurements as a function of clay concentration C_{RDS} and NIPA concentration C_{NIPA}. The normalized intermediate scattering function, $f(q,\tau)$, was calculated from the normalized time-averaged ICF, $g_T^{(2)}(q,\tau) - 1$, by eq 9, and the fluctuating component, $\langle I_F(q)\rangle_E$, was separated from the ensemble-averaged scattered intensity, $\langle I(q)\rangle_E$, by eq 8. Although $g_T^{(2)}(q,\tau) - 1$ was measured in the angular range of 40−150°, data obtained at 90° are mainly used to present the key features of the nanocomposite hydrogels and elucidate the data analysis procedure. We will omit q from the brackets in the case of $\theta = 90°$ in the following.

Effect of Clay Concentration. Figure 3 shows the variations of time-averaged scattered intensity, $\langle I\rangle_T$, with sample position (position of the scattering volume within the gel) obtained at $\theta = 90°$ for PNIPA polymerized with a C_{NIPA} of 646 mM and various C_{RDS} values at 25 °C. The solid line is the ensemble-averaged scattered intensity, $\langle I\rangle_E$, measured as described in the Experimental Section. The dashed line indicates the fluctuating component of the scattered intensity, $\langle I_F\rangle_T$, estimated by eq 8 (see below). For the PNIPA solution ($C_{RDS} = 0$), $\langle I\rangle_T$ is practically independent of sample position and $\langle I\rangle_T = \langle I\rangle_E$. On the other hand, for PNIPA/Laponite RDS nanocomposite hydrogels, $\langle I\rangle_T$ strongly fluctuates with sample positions and the typical speckle pattern appears. The excursions of the local time-averaged scattering intensity from its ensemble average rise with an increase in C_{RDS}.

As expected for a nonergodic system like the PNIPA/Laponite RDS nanocomposite hydrogels, the normalized time-averaged ICF, $g_T^{(2)}(q,\tau) - 1$, depends on the sample position. Figure 4a shows some typical examples of $g_T^{(2)}(q,\tau) - 1$, measured at $\theta = 90°$ on the sample with a C_{NIPA} of 646 mM and a C_{RDS} of 0.03 g/mL at different sample positions, i.e., different speckles. Clearly, the three curves are different, although they were measured on the same gel. Note that the tails of these curves

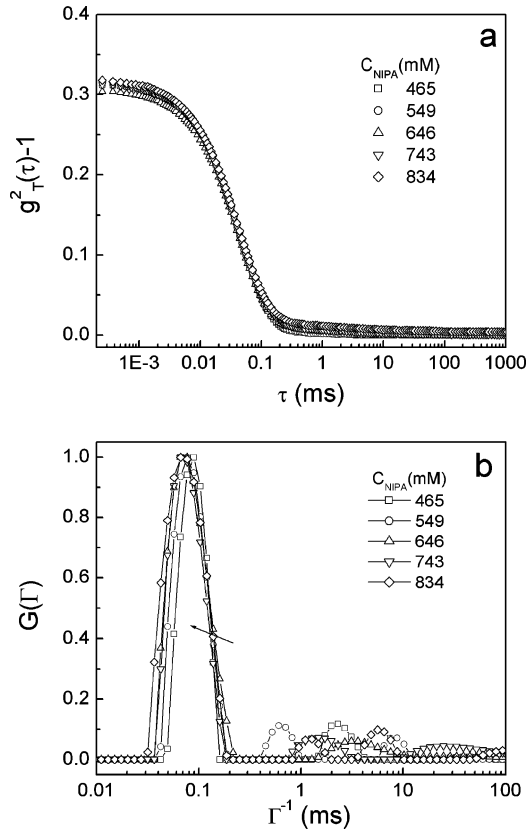

Figure 2. (a) Normalized time-averaged ICF, $g_T^{(2)}(\tau) - 1$, of solutions of linear PNIPA at various concentrations taken at a scattering angle of 90°. (b) Characteristic decay time distribution functions, $G(\Gamma)$, of the ICFs depicted in panel a. The arrow indicates the shift with an increase in concentration.

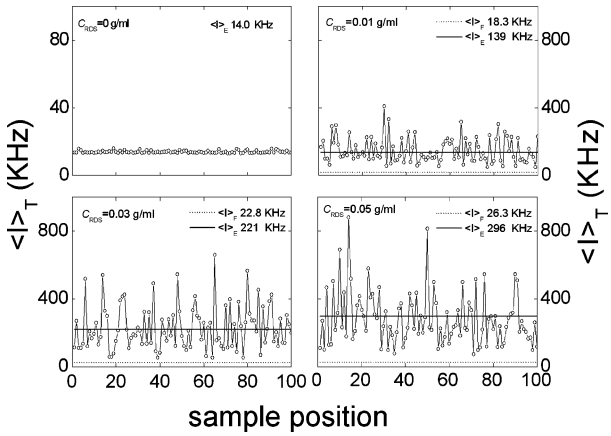

Figure 3. Variations of time-averaged scattered intensity, $\langle I\rangle_T$, with sample position, i.e., the speckle patterns, obtained at a scattering angle of 90° for a PNIPA solution and for gels with various Laponite RDS concentrations ($C_{NIPA} = 646$ mM). The solid and dashed lines indicate the ensemble averages of the scattered intensity, $\langle I\rangle_E$, and the fluctuating components of the scattered intensity, $\langle I_F\rangle_T$, respectively.

are not parallel to the time axis, indicating a very slow relaxation mode besides the fast relaxation mode. Both the fast relaxation mode and the slow relaxation mode seem to depend on sample position. The other characteristic of nonergodicity is the reduction of initial amplitude σ_I^2, which is also dependent on the sample position.

Figure 4b shows the $G(\Gamma)$ distribution functions of $g_T^{(2)}(\tau) - 1$ in Figure 4a. These $G(\Gamma)$ functions give sharp peaks, which are quite different from those of pure clay suspensions. This may indicate that the origin of the fast relaxation mode of

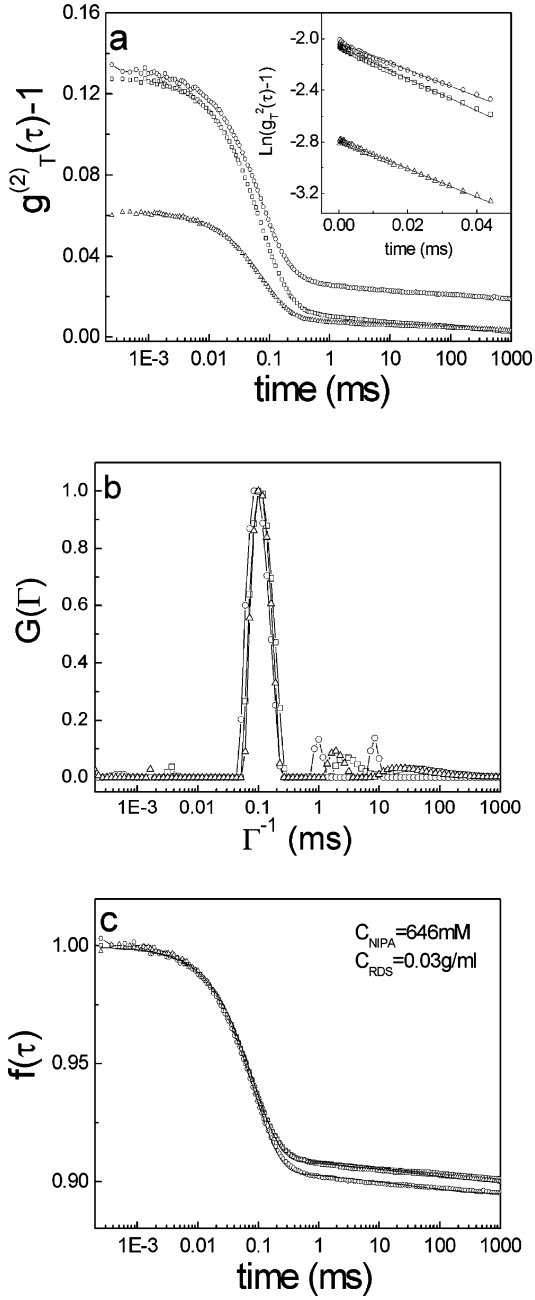

Figure 4. (a) Some typical examples of $g_T^{(2)}(\tau) - 1$, measured at $\theta = 90°$ on the sample with a C_{NIPA} of 646 mM and a C_{RDS} of 0.03 g/mL at different sample positions. The inset shows the linear fit of $\ln[g_T^{(2)}(\tau) - 1]$ vs τ in the short-time limit (cumulant analysis). (b) Distribution functions of the characteristic decay time, $G(\Gamma)$, of $g_T^{(2)}(\tau) - 1$ in panel a. (c) Normalized intermediate ensemble-averaged scattering functions, $f(\tau)$, calculated from $g_T^{(2)}(\tau)$ values given in panel a, according to eq 9. The solid lines are the best fits with eq 12. Curves in panels b and c are labeled with the same symbols as those in panel a.

nanocomposite hydrogels is very different from that of pure clay suspensions, as also reported by Shibayama et al.[28] Note that the $G(\Gamma)$ functions of the PNIPA solutions also give sharper peaks at similar decay times.

The universal features of a nonergodic system are better captured by the normalized ensemble-averaged ICF, $g_E^{(2)}(q,\tau)$, or the normalized intermediate scattering function, $f(q,\tau)$. As shown in the theoretical section, $f(q,\tau)$ can be directly calculated from the measured $g_T^{(2)}(q,\tau)$ by using eq 9, provided that $\langle I(q)\rangle_E$ and σ_I^2 are known. $\langle I(q)\rangle_E$ was experimentally measured, and σ_I^2 can be obtained by linearly fitting the plot of $\ln[g_T^{(2)}(q,\tau) - 1]$ versus τ in the short time limit (cumulant analysis), as shown in the inset of Figure 4a.[32,43]

Figure 4c shows the calculated $f(q,\tau)$ values. According to the theory derived by Pusey and van Megen, the $f(q,\tau)$ values should be identical for a given gel irrespective of the sample position. This is actually closely observed. For short times, the curves of the calculated $f(q,\tau)$ functions are practically overlapping. There is some slight variation at long times [less than 1% in $f(q,\tau)$]. Whether this is due to the limited accuracy of the measurements or has a physical reason remains to be discussed. All of the curves seem to approach a finite value of $f(q,\infty)$, indicating the existence of the frozen-in component in the nanocomposite hydrogels. Similar phenomena had been found by Joosten et al. in polyacrylamide gels with trapped colloidal particles.[32]

To estimate $f(q,\infty)$, the $f(q,\tau)$ functions were fitted with a nonlinear least-squares fitting procedure using the expression

$$f(q,\tau) = f(q,\infty) + A\exp\left(-\frac{t}{\tau_{fast}}\right) + [1 - A - f(q,\infty)]\exp\left[-\left(\frac{t}{\tau_{slow}}\right)^{\gamma}\right] \quad (12)$$

τ_{fast} and τ_{slow} are the relaxation times associated with the fast and slow relaxation modes of $f(q,\tau)$, respectively. This functional form was chosen primarily because it allows for reproducible and satisfactory fits of the data. As illustrated in Figure 4c, the fits are hardly distinguished from the data.

In general, $f(q,\infty)$ is in the range of 0.85−0.92, meaning that the greatest contribution to scattering results from the static or frozen-in structure. Prefactor A of the term corresponding to the fast fluctuations is in the range of 0.08−0.13, leaving approximately <0.02 for the prefactor of the slow mode, $1 - A - f(q,\infty)$.

The values of τ_{fast} are independent of the sample positions within experimental error. τ_{fast} also shows a q^{-2} dependence as observed for the PNIPA solutions, indicating that the fast relaxation mode is diffusive and associated with concentration fluctuations of the polymer chains in the nanocomposite hydrogels (see below for details). On the other hand, the values of τ_{slow} show a broad variation from ∼10 to 10^4 ms. They strongly depend on the sample positions and scattering vector, while the values of the exponent of the stretched exponential are essentially constant ($\gamma \approx 0.3$).

The fact that γ turns out to be practically constant justifies a discussion of the possible physical origins of the slow mode. It is not clear now why τ_{slow} should depend on the sample positions. For colloidal particles trapped in polymer gels, τ_{slow} is viewed as the characteristic exploration time of the Brownian cage, i.e., the time each particle requires to explore a significant portion of its allowed positions. Correspondingly, the values of τ_{slow} obtained from $f(q,\tau)$ functions are reported to be independent of the measured sample positions and observation scale q^{-1}.[44] However, unlike the colloidal particles trapped in the gels, the clay particles in our system behave like multifunctional cross-links in the nanocomposite hydrogels. They adsorb (or bind) a certain amount of polymer chains, forming brushlike structures with some of the chains connecting different clay particles. Therefore, the slow relaxation mode characterized by τ_{slow} may arise from cooperative motions of a number of clay particles together with the interconnecting and adsorbed polymer chains.

The observation that the values of τ_{slow} are strongly dependent on the sample positions, even though they had been obtained

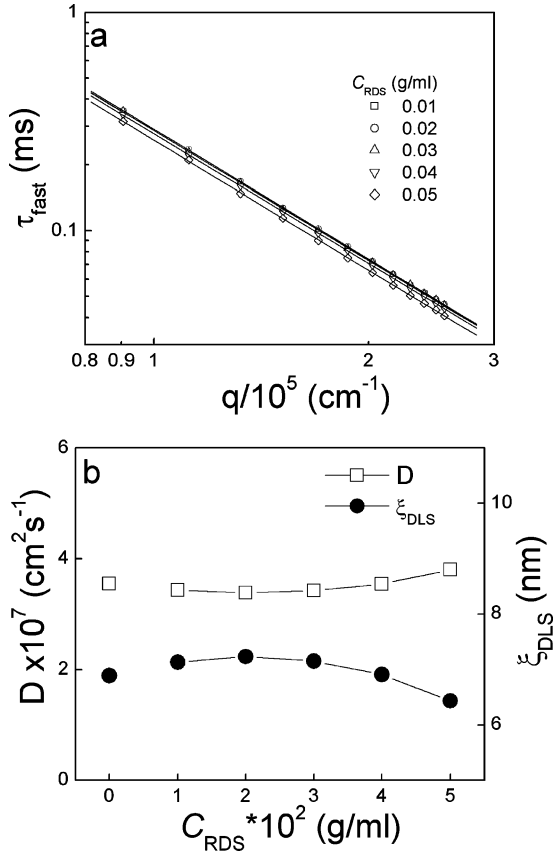

Figure 5. (a) Averaged values of τ_{fast} vs scattering vector q for the sample with a C_{NIPA} of 646 mM and various C_{RDS} values. The solid lines present the $\tau_{fast} \sim q^{-2}$ fit. (b) Diffusion coefficient D calculated from panel a by the relation $Dq^2 = 1/\tau_{fast}$ and corresponding correlation length ξ_{DLS} calculated according to eq 13 as a function of clay concentration, C_{RDS}. Note that the diffusion coefficient and correlation length of the corresponding PNIPA solution are also included.

by applying eq 9 to the normalized time-averaged ICF, implies that the slowly fluctuating component is not appropriately treated within the model of Pusey and van Megen. There might be a coupling between the slowly fluctuating component and static inhomogeneities. It should be kept in mind, however, that the slowly fluctuating component is the least significant contribution to total scattering. Thus, we will focus our discussions on the fast mode as well as the separation of the fluctuating component, $\langle I_F(q)\rangle_T$, and the frozen-in component, $f(q,\infty)$, in the following.

Figure 5a shows the values of τ_{fast} as a function of scattering vector q for the nanocomposite hydrogels with various clay concentrations. Note that the values of τ_{fast} were averaged over all of the measured sample positions for a given q. The solid lines in Figure 5a show that τ_{fast} scales as $q^{-2.0}$, indicating that the fast mode is purely diffusive. The diffusion coefficient, D, obtained from these fits can be related to the correlation length of the nanocomposite hydrogel, ξ_{DLS}, via the Stokes−Einstein equation

$$\xi_{DLS} = \frac{k_B T}{6\pi\eta_s D} \tag{13}$$

where $\eta_s = 0.89$ mPa for water. The obtained D and ξ_{DLS} are shown in Figure 5b. ξ_{DLS}, being a measure of the characteristic length scale of the dynamic network, is in the same range as that of a PNIPA solution. It seems to decrease slightly with the increase in the clay concentration, C_{RDS}. An increasing C_{RDS} (with a fixed C_{NIPA}) leads to an increase in the cross-link density

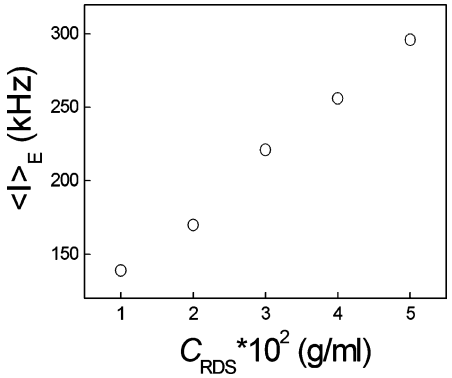

Figure 6. Ensemble-averaged scattered intensity, $\langle I\rangle_E$, obtained at $\theta = 90°$ as a function of clay concentration, C_{RDS} ($C_{NIPA} = 646$ mM).

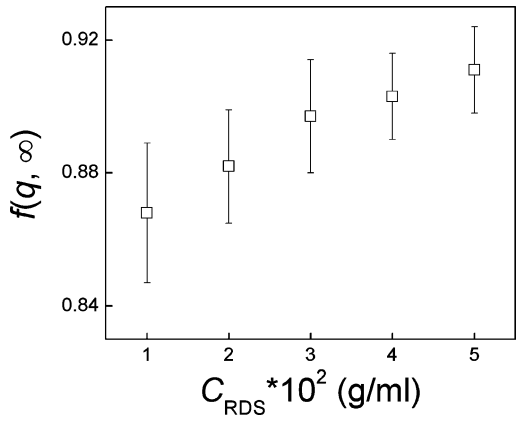

Figure 7. Frozen-in (or static) component $f(q,\infty)$ obtained at $\theta = 90°$ as a function of clay concentration, C_{RDS} ($C_{NIPA} = 646$ mM). Note that the $f(q,\infty)$ values were averaged over 100 sample positions.

of the PNIPA/Laponite RDS nanocomposite hydrogel and a reduction of its mesh size.[29] These results agree well with those observed in chemically cross-linked PNIPA hydrogels and PNIPA/Laponite XLG nanocomposite hydrogels.[9,28]

The scattered intensity of the PNIPA/Laponite RDS nanocomposite hydrogels shows a marked angular dependence with a strong upturn in the lower q range. This strong q dependence was systematically investigated and discussed in a previous paper.[29] Here, we focus on the value of $\langle I(q)\rangle_E$ obtained at $\theta = 90°$ and how it is composed of fluctuating and nonfluctuating contributions. Figure 6 shows that the ensemble-averaged scattered intensity, $\langle I\rangle_E$, increases rapidly with an increase in C_{RDS}. In parallel, $f(q,\infty)$, the frozen-in fraction of $\langle I\rangle_E$, is also increasing gently with the increase in C_{RDS} (Figure 7). This behavior seems reasonable: The clay particles behave as multifunctional cross-links. After polymerization, the clay particles are relatively fixed by the adsorbed or cross-linked polymer chains and cannot diffuse through the medium. But they still scatter the laser light strongly, thus giving rise to the frozen-in component. On the other hand, the increase in C_{RDS} also leads to an increase in the spatial inhomogeneity of PNIPA, which increases the ensemble-averaged scattered intensity as well.

The fluctuating component $\langle I_F(q)\rangle_T$ was obtained with eq 8. Inspection of its angular dependence revealed that $\langle I_F(q)\rangle_T \sin(\theta)$ is independent of q within experimental error [multiplication with $\sin(\theta)$ just normalizes the scattering volume]. This result is another indication of the fact that the dynamic part of the density fluctuations has a correlation range much smaller than the wavelength of the light,[33] in full agreement with the data for ξ_{DLS} represented in Figure 5b.

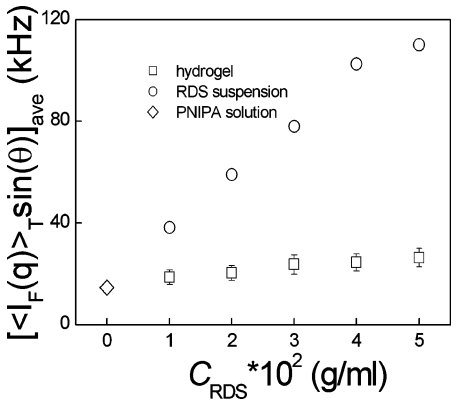

Figure 8. Averaged fluctuating component, $[\langle I_F(q)\rangle_T \sin(\theta)]_{ave}$, for PNIPA/Laponite nanocomposite hydrogels with a C_{NIPA} of 646 mM (□), the corresponding PNIPA solution (◇), and the pure Laponite RDS suspensions (○).

The fluctuating component $\langle I_F(q)\rangle_T \sin(\theta)$, averaged over all sample positions and over the full angular range (θ from 40 to 150°) for a given gel, is shown in Figure 8 as a function of clay concentration. The amplitude of the fluctuating component increases slightly with C_{RDS}, which is similar to the results observed in chemically cross-linked polyacrylamide hydrogels,[33] whereas for chemically cross-linked PNIPA hydrogels, Shibayama et al. reported that the fluctuating component of the scattered intensity is independent of the cross-link density.[9] In contrast to the chemically cross-linked polymer hydrogels, the cross-linker used here is Laponite RDS particles, which are themselves strong scattering centers. Accordingly, the fluctuating component of the scattered intensity of the PNIPA/Laponite RDS nanocomposite hydrogels may have two contributions, i.e., from PNIPA chains and from the Laponite RDS particles. Also shown in Figure 8 are the scattering intensity of a corresponding PNIPA solution and the scattering intensities of Laponite RDS suspensions. The comparison reveals that the scattering intensities of the clay suspensions are much larger than the fluctuating component of the scattering intensities of the nanocomposite hydrogels. This means that, upon network formation, the clay particles are largely or completely immobilized so that they do not contribute significantly to the fluctuating scattering component but give rise to the static or frozen-in component. The reason for this behavior is their being tied to a fairly large number of polymer chains. The slight increase in the fluctuating scattering component of the gels with rising clay concentration, which is still observed, may then be attributed to some remaining, drastically reduced mobility of the clay particles. On the other hand, we cannot exclude the possibility that it is due to the polymer chains which show a different behavior in the network and in solution. With a larger amount of clay, the portion of PNIPA adsorbed at its surface is increased. Therefore, the polymer concentration in that part of the system where fluctuations mainly occur (away from the clay surface) is reduced. This heterogeneous concentration distribution may also result in an increase in the fluctuating scattering component.

Effect of Monomer Concentration. Figure 9 shows the variations of time-averaged scattered intensity $\langle I\rangle_T$ with sample position obtained at $\theta = 90°$ for PNIPA/Laponite RDS nanocomposite hydrogels with a C_{RDS} of 0.03 g/mL and various C_{NIPA} values. The solid and dashed lines represent the ensemble average of the scattered intensity, $\langle I\rangle_E$, and the fluctuating component of the scattered intensity, $\langle I_F\rangle_T$, respectively. For the pure Laponite RDS suspension, $\langle I\rangle_T$ is independent of sample position and $\langle I\rangle_T \approx \langle I\rangle_E$, while for the PNIPA/Laponite RDS

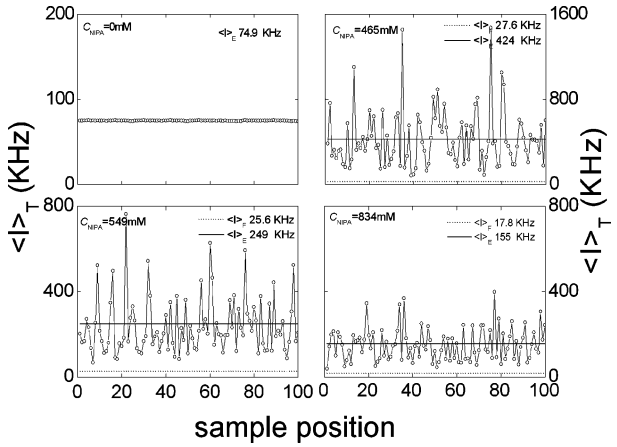

Figure 9. Variations of time-averaged scattered intensity, $\langle I\rangle_T$, with sample position, i.e., the speckle patterns, obtained at a scattering angle of 90° for a clay suspension and for gels with various monomer concentrations ($C_{RDS} = 0.03$ g/mL). The solid and dashed lines indicate the ensemble averages of the scattered intensity, $\langle I\rangle_E$, and the fluctuating components of the scattered intensity, $\langle I_F\rangle_T$, respectively.

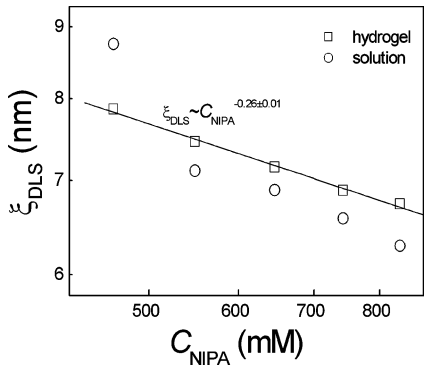

Figure 10. Dynamic correlation length ξ_{DLS} obtained for PNIPA/clay nanocomposite hydrogels (□) and the corresponding PNIPA solutions (○) as a function of monomer concentration (log−log scale). The solid line is a linear fit to the gel data.

hydrogels, $\langle I\rangle_T$ strongly fluctuates with sample positions. The speckle pattern decreases with an increase in C_{NIPA} when the other preparation parameters are fixed.

The normalized intermediate ensemble-averaged scattering functions, $f(q,\tau)$, were calculated and analyzed in the way described above. Similar results were obtained for the values of τ_{slow} and γ used to characterize the slow relaxation mode. The values of τ_{slow} are position-dependent. The values of γ are independent of sample position, monomer concentration, and scattering vector q (data not shown). The fast mode of $f(q,\tau)$ is also found to be purely diffusive, i.e., $\tau_{fast} \sim q^{-2.0}$.

Figure 10 shows the correlation lengths, ξ_{DLS}, of the fast relaxation mode of the gels and, for comparison, those of the corresponding PNIPA solutions. There is practically no difference between gels and solutions with regard to ξ_{DLS}. For both systems, ξ_{DLS} decreases with the increase in monomer concentration. According to the scaling theory, the correlation length for semidilute polymer solutions in an athermal solvent is expected to scale as $C^{-3/4}$.[45] The data obtained for the clay/PNIPA nanocomposite hydrogels are well described by the relation $\xi_{DLS} \sim C_{NIPA}^{-0.26\pm0.01}$, whereas the exponent for the PNIPA solutions may or may not be somewhat larger, depending on how the first data point is counted. Several authors have observed a scaling relation between ξ_{DLS} and the concentration of the monomer for polyacrylamide solutions as well as hydrogels. For polyacrylamide solutions, an exponent of −0.27

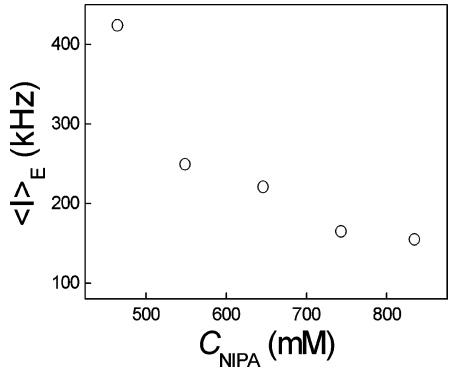

Figure 11. Ensemble-averaged scattered intensity, $\langle I \rangle_E$, obtained at $\theta = 90°$ as a function of monomer concentration, C_{NIPA} ($C_{RDS} = 0.03$ g/mL).

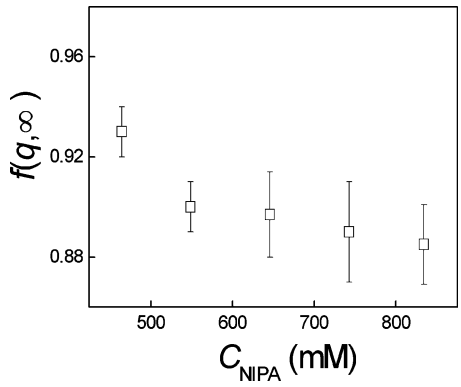

Figure 12. Frozen-in component $f(q,\infty)$ obtained at $\theta = 90°$ as a function of monomer concentration, C_{NIPA} ($C_{RDS} = 0.03$ g/mL). Note that the $f(q,\infty)$ values were averaged over 100 sample positions.

was reported by Joosten et al.,[33] while a value of -0.56 was found by Sellen.[46,47] Exponents of around -0.6 were reported for polyacrylamide hydrogels with fixed cross-link density.[33] Our data seem to agree with the general trend of the other experiments in that the concentration dependence is weaker than that predicted by scaling theory. However, the concentration range covered is rather narrow, and this observation should not be overemphasized.

Figure 11 shows the ensemble-averaged scattered intensity, $\langle I \rangle_E$, as a function of C_{NIPA}, while Figure 12 represents the pertinent fraction of the static compoent, $f(q,\infty)$, both quantities obtained at $\theta = 90°$. $f(q,\infty)$ is around 0.9; hence, 90% of the ensemble-averaged scattering intensity shown in Figure 11 corresponds to the static component. With an increase in C_{NIPA}, the spatial inhomogeneities of the PNIPA/Laponite RDS nanocomposite hydrogel are reduced, and this leads to a decrease in the static component of the scattering intensity. This point was discussed in detail in ref 29, where the angular dependence was also taken into account. Here we confine ourselves to state that those results are clearly confirmed by DLS experiments.

The fluctuating component, $\langle I_F(q) \rangle_T \sin(\theta)$, is independent of q within experimental error. Figure 13 shows, like Figure 8, the fluctuating component, $\langle I_F(q) \rangle_T \sin(\theta)$, averaged over all sample positions and the full angular range (θ from 40° to 150°), as a function of C_{NIPA}. $\langle I_F(q) \rangle_T \sin(\theta)$ decreases somewhat with an increase in C_{NIPA}, an observation also made with chemically cross-linked PNIPA hydrogels.[48] Also shown in Figure 13 are the corresponding scattering intensities of PNIPA solutions having the same concentration, and that of the clay suspension. The fact that the fluctuating component of the gels is far less than the scattering intensity of the pure clay suspension confirms

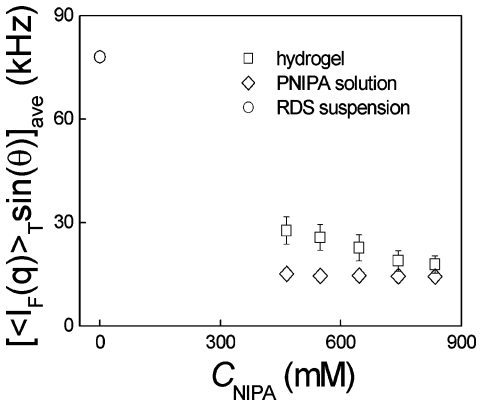

Figure 13. Averaged fluctuating component $[\langle I_F(q) \rangle_T \sin(\theta)]_{ave}$ for the PNIPA/Laponite nanocomposite hydrogels with a C_{RDS} of 0.03 g/mL (□), the corresponding PNIPA solutions (◇), and the corresponding pure Laponite RDS suspension (○).

the view that the thermal fluctuations of the clay particles are largely suppressed upon formation of the nanocomposite hydrogels. The second important fact observed in Figure 13 is that the fluctuating component of the gels is definitely larger than the scattering intensity of the PNIPA solutions, the gap between the two increasing with a lower NIPA concentration. As discussed above, the fluctuating component of the scattered intensity of the PNIPA/Laponite RDS nanocomposite hydrogels may originate from two contributions: from polymer chains which may exhibit a different behavior in gels and solutions and from some residual mobility of the clay particles. As reported previously, the number of elastically effective network chains per clay particle, f_{eff}, is proportional to the concentration of the monomer when the other preparation parameters are fixed. It seems conceivable that the level of suppression of thermal fluctuations of the clay particles increases with the number of network chains tied to one particle. Therefore, the roughly linear dependence of $\langle I_F(q) \rangle_T \sin(\theta)$ on C_{NIPA} depicted in Figure 13 is consistent with the view that it originates from a contribution of the PNIPA chains, this part being similar to that of a corresponding solution, plus a second contribution arising from the residual mobility of the clay particles. The latter is dependent on how well the clay particles are tied to the network.

Conclusions

The spatial inhomogeneity and the chain dynamics of PNIPA/Laponite RDS nanocomposite hydrogels, obtained by polymerizing NIPA in a suspension of exfoliated clay particles, were investigated by dynamic light scattering. Particular emphasis was placed on a systematic variation of the preparation conditions, i.e., clay concentration C_{RDS} and monomer concentration C_{NIPA}. A speckle pattern typical of a nonergodic system was observed, clearly indicating the formation of a network structure even in the absence of chemical cross-links. The excursions of the local time-averaged scattering intensity from its ensemble average, serving as a measure of spatial inhomogeneity, increase with an increase in C_{RDS} and decrease with an increase in C_{NIPA} when the other preparation parameters are fixed.

The application of the Pusey and van Megen procedure to dynamic light scattering data allows the separation of the total scattering intensity into a fluctuating and a static or frozen-in component. The static component is by far the dominant one. It increases strongly with an increase in C_{RDS} and drops with an increase in C_{NIPA}. The major part of it is due to the clay particles, which become relatively fixed at certain locations in

space after network formation and are strongly scattering the light. Since each clay particle is tied to some 50 adsorbed or bound network chains (cf. ref 29), its mobility is largely suppressed. This conclusion is supported by the observation that the strong fluctuating scattering component of a clay suspension vanishes upon gelation, and instead, a strong static component appears.

The fluctuating component, which amounts to ∼10% of the total scattering, can be broken down into two relaxation processes. The fast mode is diffusive in nature and can be related to a dynamic correlation length of 6−8 nm. This length scale is the same as that of a PNIPA solution. The longer relaxation time of the second (minor) mode, modeled as a stretched exponential, varies appreciably with sample position. Such a second relaxation has been observed only with gels which are cross-linked via clay particles; it does not appear in chemically cross-linked systems. One may conjecture that the slow fluctuating mode has an origin similar to that of the longer static correlation length (200−250 nm) deduced from the strong angular dependence of scattering intensity reported in ref 29. Both phenomena point to large-scale structures and are peculiar to particle-cross-linked systems.

The intensity of the fluctuating component as a whole is somewhat larger than that of a corresponding PNIPA solution. It increases slightly with an increase in the clay content and is reduced when the NIPA concentration is increased. Both observations lead to the conclusion that the amount of the intensity exceeding that of a PNIPA solution is due to some residual mobility of the clay particles. This residual mobility depends on how tightly the clay particles are fixed in the network and therefore varies in proportion with the C_{RDS}/C_{NIPA} ratio.

Acknowledgment. B.D. thanks the Alexander von Humboldt Foundation for financial support.

References and Notes

(1) Ruel-Gariepy, E.; Leroux, J. C. *Eur. J. Pharm. Biopharm*. **2004**, *58*, 409−426.
(2) Okano, T. *Adv. Polym. Sci*. **1993**, *110*, 180.
(3) Johnson, B. D.; Beebe, D. J.; Crone, W. *Mater. Sci. Eng., C* **2004**, *24*, 575−581.
(4) Varga, Z.; Feher, J.; Filipcsei, G.; Zrinyi, M. *Macromol. Symp*. **2003**, *200*, 93−100.
(5) Doing, L. C.; Hoffman, A. S. *J. Controlled Release* **1986**, *31*, 7328.
(6) Jeong, B.; Gutowska, A. *Trends Biotechnol.* **2002**, *20*, 305−311.
(7) Stayton, P. S.; Shimoboji, T.; Long, C.; Chilkoti, A.; Chen, G.; Harris, J. M.; Hoffman, A. S. *Nature* **1995**, *378*, 472−474.
(8) Ikkai, F.; Shibayama, M. *J. Polym. Sci., Part B* **2005**, *43*, 617−628.
(9) Shibayama, M.; Norisuye, T.; Nomura, S. *Macromolecules* **1996**, *29*, 8746−8750.
(10) Shibayama, M.; Takata, S.; Norisuye, T. *Physica A* **1998**, *249*, 245−252.
(11) Norisuye, T.; Kida, Y.; Masui, N.; Tran-Cong-Miyata, Q.; Maekawa, Y.; Yoshida, M.; Shibayama, M. *Macromolecules* **2003**, *36*, 6202−6212.
(12) Takata, S.; Norisuye, T.; Shibayama, M. *Macromolecules* **2002**, *35*, 4779−4784.
(13) Sayil, C.; Okay, O. *Polym. Bull*. **2000**, *45*, 175−182.
(14) Sayil, C.; Okay, O. *Polymer* **2001**, *42*, 7639−7652.
(15) Kizilay, M. Y.; Okay, O. *Macromolecules* **2003**, *36*, 6856−6862.
(16) Nie, J.; Du, B.; Oppermann, W. *Macromolecules* **2004**, *37*, 6558.
(17) Schröder, U. P.; Oppermann, W. In *The Physical Properties of Polymer Gels*; Cohen Addad, J. P., Ed.; John Wiley: New York, 1996; Chapter 2, pp 19−38.
(18) Ravi, N.; Mitra, M.; Hamilton, P.; Horkay, F. *J. Polym. Sci., Part B: Polym. Phys.* **2002**, *40*, 2677.
(19) Horkay, F.; Basser, P. J.; Hecht, A. M.; Geissler, E. *Polymer* **2005**, *46*, 4242−4247.
(20) Lin-Gibson, S.; Bencherif, S.; Antonucci, J. M.; Jones, R. L.; Horkay, F. *Macromol. Symp*. **2005**, *227*, 243−254.
(21) Messersmith, P. B.; Znidarsich, F. Nanophase and Nanocomposite materials II. In *MRS Symposium Proceedings 457*; Komarneni, S., Parker, J. C., Wollenberger, H. J., Eds.; Materials Research Society: Pittsburgh, PA, 1997; p 507.
(22) Xia, X.; Yih, J.; D'Souza, N. A. D.; Hu, Z. *Polymer* **2003**, *44*, 3389−3393.
(23) Liang, L.; Liu, J.; Gong, X. *Langmuir* **2000**, *16*, 9895−9899.
(24) Haraguchi, K.; Takeshita, T. *Adv. Mater*. **2002**, *14*, 1121.
(25) Haraguchi, K.; Takeshita, T.; Fan, S. *Macromolecules* **2002**, *35*, 10162.
(26) Haraguchi, K.; Farnworth, R.; Ohbayashi, A.; Takeshita, T. *Macromolecules* **2003**, *36*, 5732.
(27) Schmidt, D.; Shah, D.; Giannelis, E. P. *Curr. Opin. Solid State Mater. Sci.* **2002**, *6*, 205−212.
(28) Shibayama, M.; Suda, J.; Karino, T.; Okabe, S.; Takehisa, T.; Haraguchi, K. *Macromolecules* **2004**, *37*, 9606.
(29) Nie, J.; Du, B.; Oppermann, W. *Macromolecules* **2005**, *38*, 5729.
(30) Haraguchi, K.; Li, H. J.; Matsuda, K.; Takehisa, T.; Elliott, E. *Macromolecules* **2005**, *38*, 3482.
(31) Pusey, P. N.; van Megen, W. *Physica A* **1989**, *157*, 705.
(32) Joosten, J. G. H.; Gelade, E. T. F.; Pusey, P. N. *Phys. Rev. A* **1990**, *42*, 2161.
(33) Joosten, J. G. H.; McCarthy, J. L.; Pusey, P. N. *Macromolecules* **1991**, *24*, 6690.
(34) Shibayama, M. *Macromol. Chem. Phys*. **1998**, *199*, 1.
(35) Fang, L.; Brown, W. *Macromolecules* **1992**, *25*, 6897.
(36) Tanaka, T.; Hocker, L. O.; Benedek, G. B. *J. Chem. Phys*. **1973**, *59*, 5151.
(37) Rodd, A. B.; Dunstan, D. E.; Boger, D. V.; Schmidt, J.; Burchard, W. *Macromolecules* **2001**, *34*, 3339.
(38) Berne, B. J.; Pecora, R. In *Dynamic Light Scattering*; Wiley: New York, 1976.
(39) Ngai, T.; Wu, C.; Chen, Y. *J. Phys. Chem. B* **2004**, *108*, 5532.
(40) Castelletto, V.; Ansari, I. A.; Hamley, I. W. *Macromolecules* **2003**, *36*, 1694.
(41) Shibayama, M.; Tanaka, T.; Han, C. C. *J. Chem. Phys.* **1992**, *97*, 6829.
(42) Shibayama, M.; Tanaka, T. *J. Chem. Phys*. **1995**, *102*, 9392.
(43) Koppel, D. E. *J. Chem. Phys*. **1972**, *57*, 4814.
(44) Nisato, G.; Hebraud, P.; Munch, J. P.; Candau, S. J. *Phys. Rev. E* **2000**, *61*, 2879.
(45) de Gennes, P. G. In *Scaling Concepts in Polymer Physics*; Cornell University: Ithaca, NY, 1979; p 80.
(46) Sellen, D. B. *J. Polym. Sci., Polym. Phys. Ed*. **1987**, *25*, 699−716.
(47) Geissler, E.; Hecht, A. M. *Macromolecules* **1981**, *14*, 185.
(48) Takeda, M.; Norisuye, T.; Shibayama, M. *Macromolecules* **2000**, *33*, 2909.